

Article

CO₂ Electrochemical Reduction by Exohedral N-Pyridine Decorated Metal-Free Carbon Nanotubes

Giulia Tuci¹, Jonathan Filippi¹, Andrea Rossin¹ , Lapo Luconi¹, Cuong Pham-Huu^{2,*}, Dmitry Yakhvarov³ , Francesco Vizza^{1,*}  and Giuliano Giambastiani^{1,2,3,*} 

¹ Institute of Chemistry of OrganoMetallic Compounds (ICCOM-CNR) and Consorzio INSTM, Via Madonna del Piano, 10-50019 Sesto F.no, Florence, Italy; giulia.tuci@iccom.cnr.it (G.T.); jonathan.filippi@iccom.cnr.it (J.F.); a.rossin@iccom.cnr.it (A.R.); lapo.luconi@iccom.cnr.it (L.L.)

² Institute of Chemistry and Processes for Energy, Environment and Health (ICPEES), UMR 7515 CNRS-University of Strasbourg (UdS), 25, rue Becquerel, CEDEX 02, 67087 Strasbourg, France

³ Alexander Butlerov Institute of Chemistry, Kazan Federal University, 420008 Kazan, Russia; yakhvar@iopc.ru

* Correspondence: cuong.pham-huu@unistra.fr (C.P.-H.); francesco.vizza@iccom.cnr.it (F.V.); giuliano.giambastiani@iccom.cnr.it or giambastiani@unistra.fr (G.G.)

Received: 1 May 2020; Accepted: 21 May 2020; Published: 28 May 2020



Abstract: Electrochemical CO₂ reduction reaction (CO₂RR) to fuels and chemicals represents nowadays one of the most challenging solutions for renewable energy storage and utilization. Among the possible reaction pathways, CO₂-to-CO conversion is the first (2e⁻) reduction step towards the production of a key-feedstock that holds great relevance for chemical industry. In this report we describe the electrocatalytic CO₂-to-CO reduction by a series of tailored N-decorated carbon nanotubes to be employed as chemoselective metal-free electrocatalysts. The choice of an exohedral functionalization tool for the introduction of defined N-groups at the outer surface of carbon nanomaterials warrants a unique control on N-configuration and electronic charge density distribution at the dangling heterocycles. A comparative electrochemical screening of variably N-substituted carbon nanomaterials in CO₂RR together with an analysis of the electronic charge density distribution at each heterocycle have suggested the existence of a coherent descriptor for the catalyst's CO faradaic efficiency (FE_{CO}). Evidence allows to infer that N-configuration (N-pyridinic vs. N-pyrrolic) of exohedral dopants and electronic charge density distribution at the N-neighboring carbon atoms of each heterocycle are directly engaged in the activation and stabilization of CO₂ and its reduction intermediates.

Keywords: CO₂ reduction reaction (CO₂RR); metal-free electrocatalysts; pyridine nuclei; exohedral chemical grafting; multi-walled carbon nanotubes

1. Introduction

The steady state increase of CO₂ concentration in the atmosphere caused by all main anthropic activities (including the massive employ of fossil fuels), is largely responsible of global warming effects and associated environmental issues such as climate changes, sea level rise and ocean acidification; phenomena that are seriously affecting our lifestyle. Accordingly, the development of new (electro)chemical technologies for CO₂ conversion into products or energy-vectors of added value represents an effective “two-birds one-stone” approach for mitigating climate effects and supplying the growing energy demand to our modern society [1,2]. One promising approach to reduce CO₂ emissions while fostering the transition towards a carbon neutral economy is given by the electrochemical CO₂ reduction reaction (CO₂RR) into chemicals to be stored, transported and used on demand [3,4]. CO₂RR holds great expectations because of its generally mild operating conditions together with the

possibility to control the reduction products (i.e., CO, formic acid, alcohols, acetic acid and small hydrocarbons) through the judicious tuning of the potentials applied to the electrochemical cell. Moreover, electrochemical devices powered by electricity generated from renewable sources such as wind, solar and hydro power contribute to make the transformation even more sustainable [5]. Despite the high energetic and environmental significance of CO₂ electroreduction, the chemical inertness of CO₂ generally requires high applied overpotentials to proceed with its electrochemical conversion. At the same time, the main competing process at work in aqueous electrolytes [hydrogen evolution reaction–HER] easily occurs under the thermodynamic potentials at which CO₂ electroreduction occurs. This side-reaction deeply affects the overall process efficiency [6]. In addition, the occurrence of multiple electron transfers under CO₂RR conditions and their close thermodynamic redox potentials [7,8] are at the origin of a generally poor process selectivity. As a result, the development of highly efficient and selective electrocatalysts for the process remains a challenging matter, partially addressed only for selected electroreduction products. Selective CO₂ electroreduction to carbon monoxide (CO) is a strategic process [9] to produce a syngas component that is exploited for the synthesis of a series of useful organic chemical products and intermediates [10]. In contrast with highly endothermic and energy demanding transformations such as the reverse water-gas-shift (rWGS) reaction [11], the selective CO₂-to-CO reduction can be achieved electrochemically already at ambient conditions with renewable energy sources. The latter reduction is a 2-protons/2-electrons process [12] where CO₂ is firstly reductively adsorbed at the catalyst surface to give an intermediate that undergoes a second proton-coupled electron transfer to give CO (and H₂O) that desorbs from the catalyst. Accordingly, an ideal electrocatalyst for the process should facilitate CO₂ surface adsorption/activation while favoring the rapid CO desorption from its surface.

Over the last decades, great efforts in this area have been devoted mainly to the design, synthesis and use of metal-containing catalysts [13–18]. However, their production costs and their sensitivity to poisoning/deactivation, together with often moderate performance in terms of process activity and selectivity, have limited their widespread application in electrocatalysis. New electrocatalytic materials including single-phase nitrogen doped carbons have recently emerged as valuable alternative to metal-based systems [19] with comparable performance in CO₂ reduction along with markedly reduced material costs [20]. Studies in the field of metal-free electrocatalysts have shown how the inclusion (doping) of light elements (i.e., N, B, S) in structure of graphitic nanocarbons improves their CO₂RR performance compared to pristine pure-carbon counterparts. Indeed, doping alters the material electronic properties and changes the carbon network morphology, thus creating high-energy surface sites that facilitate CO₂ interaction and foster its subsequent electrochemical conversion [21]. To date, various N-doped nanocarbons have been successfully applied as electrocatalysts for the CO₂ conversion to get target products such as CO [22–29], formic acid (HCOOH) [30–32] or acetic acid (CH₃CO₂H) [33]. Despite these achievements, the nature of the active sites directly engaged in CO₂ activation/conversion remains rather elusive and the generally complex nature of all synthesized N-doped carbon nanomaterials hampers a definitive comprehension of the structure-composition-reactivity relationships at the origin of their catalytic performance. The co-existence of different N-configurations (i.e., pyridinic, quaternary, pyrrolic) in classically chemical-vapor-deposition (CVD)-prepared N-doped nanocarbons together with the presence of metal traces coming from the experimental conditions applied to their production have raised serious debates within the scientific community on the nature of the active species for the process, leading to often conflicting experimental and theoretical results [19,21–24,26–28,34–36] (For classically N-doped nanocarbons where pyridinic-N sites are claimed to be responsible for CO₂RR performance to CO, see: [26,27,36]. For classically N-doped nanocarbons where graphitic-N atoms are claimed to be responsible for CO₂RR performance to CO, see: [21,28]. For classically N-doped nanocarbons where pyridinic and graphitic-N atoms are claimed to be responsible for CO₂RR performance to CO, see: [19,23]. For classically N-doped nanocarbons where neighbouring C-atoms to N-sites or C-N polarized bonds are claimed to be responsible for CO₂RR performance to CO, see: [22].). We have recently reported on

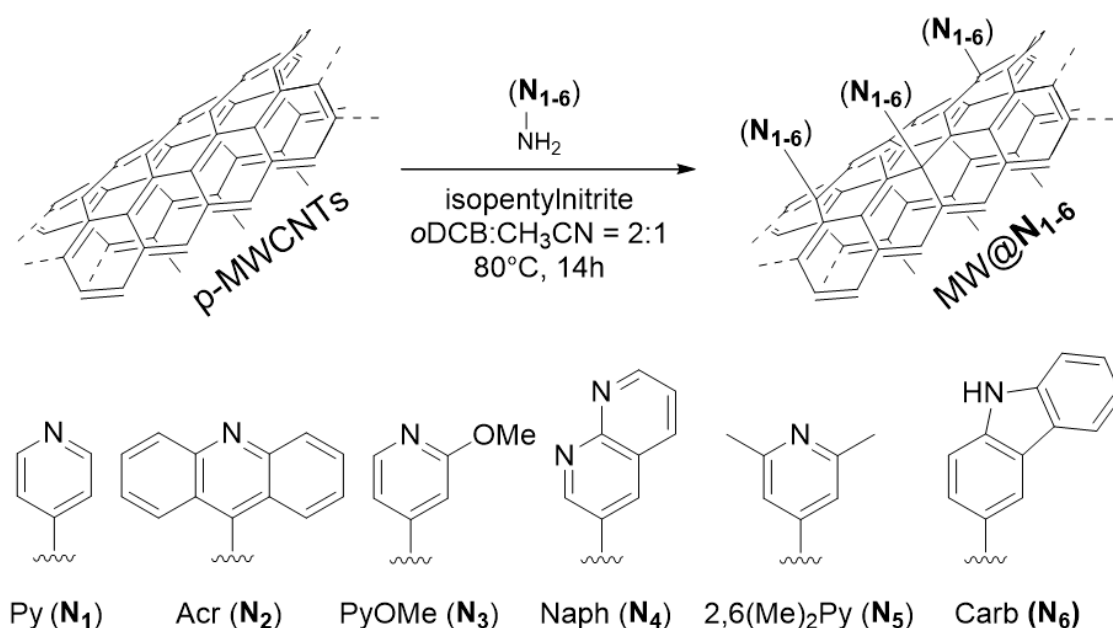
the role of aziridine-decorated carbon nanotubes as highly efficient and chemoselective electrocatalysts for the CO₂-to-CO conversion [37]. The use of an exohedral functionalization strategy for the *ad-hoc* introduction of surface exposed N-containing functionalities [38–43] has contributed to clarify the role of selected N-containing groups towards CO₂ activation and its electrochemical conversion. Tailored N-functionalized catalysts provide a useful tool for the comprehension of the CO₂RR mechanism at work on these metal-free systems and offer an ideal platform to rule out any conflicting or synergistic contribution raising from the presence of residual metal traces.

Since pyridine nuclei are commonly recognized among the most active sites for CO₂RR in more conventionally prepared N-doped nanocarbons [19,26–28], in this paper we focused on a series of N-pyridinic heterocycles as dangling groups covalently linked at the surface of multi-walled carbon nanotubes to be employed as metal-free electrocatalysts. The comparative study unveils the role of pyridinic nuclei for the process, suggesting the existence of a coherent descriptor for the catalyst selectivity towards CO (faradaic efficiency, FE_{CO}) based on the electronic charge density distribution at the carbon atoms neighboring N-sites of the variably substituted heterocycles. In line with related studies from the literature [31,44], our conclusions support the key role played by N-neighboring carbon atoms on the CO₂ activation mechanism operative with these metal-free electrocatalysts.

2. Materials and Methods

Multi-walled carbon nanotubes (MWCNTs-98% in C) were obtained from Sigma-Aldrich (Lot# MKBH5814V) and used as received. Unless otherwise stated, all other chemicals were purchased from commercial suppliers and used as received without further purification. Samples sonication was conducted on an Elma S15 Elmasonic sonicator bath (37 kHz) while cooling samples in a water/ice mixture throughout the treatment. Samples MW@N_{1–4} and MW@N₆ (Scheme 1) used in the study have been prepared according to literature procedures [38,41,43] and characterized in terms of N-loading (elemental analysis and acid-base titration) and N-configuration (X-ray photoelectron spectroscopy—XPS) as to confirm their ultimate identity. The new sample MW@N₅ (Scheme 1) was prepared following a general procedure for the exohedral MW-functionalization via aryldiazonium salt chemistry. The functionalization protocol was similar to that already used for the other samples and described hereafter in brief for the sake of completeness. MWCNTs (80 mg) were weighed into a two-necked 150 mL flask and suspended in 65 mL of dry and degassed oDCB (ortho-dichlorobenzene). After sonication for 30 min in an ultrasonic bath, a solution of 4-amino-2,6-dimethylpyridine (1.72 mmol) in dry and degassed acetonitrile (30 mL) and isopentyl nitrite (0.35 mL, 2.58 mmol) were added in sequence and the suspension was additionally sonicated for 10 min. Afterwards, the stirred mixture was heated up to 80 °C for 14 h before being cooled down to room temperature, diluted with ethylacetate (20 mL) and sonicated for 20 min. The solid residue was then recovered by centrifugation/washing/decantation procedure using ethylacetate (20 mL) and dichloromethane (twice 15 mL) as solvent. The solid residue was finally suspended in dichloromethane, sonicated for 15 min and filtered through a 0.2 µm-pore PTFE filter. MW@N₅ was finally dried at 50 °C under vacuum to constant weight and stored on air at room temperature. X-ray Photoelectron Spectroscopy (XPS) measurements were conducted on a Thermo-VG scientific spectrometer, operating in ultrahigh vacuum (UHV) and equipped with a CLAM4 (Multiplier Channel Detector—MCD) hemispherical electron analyzer. The Al K α line (1486.6 eV) of a dual anode X-ray source was used as incident radiation. Charge correction of the spectra was performed by taking the sp² graphitic component of the C 1s spectrum as internal reference (Binding Energy, BE = 284.6 eV). Survey and high-resolution spectra were recorded in constant pass energy mode (100 and 20 eV, respectively). High resolution spectra of detected elements were acquired for semi-quantitative and detailed BE chemical shift analysis. The high-resolution spectra were fitted with mixed Gaussian-Lorentzian peaks after a Shirley background subtraction. The determined standard deviation in the peak position was ± 0.2 eV. Atomic percentages were calculated using the corresponding core level peaks properly normalized to the photoemission cross section and assuming a homogeneous distribution arrangement model. Elemental analyses were

carried out on a Thermo FlashEA 1112 Series CHNS-O elemental analyzer and elemental average values were calculated over three independent runs. *Acid-base titration* was conducted as follows: 5 mg of MW@N₁₋₅ were suspended in 7 mL of a HCl standard solution (2.8×10^{-3} M, standardized with Na₂CO₃ as primary standard), sonicated for 30 min and stirred at room temperature for 48 h. Afterwards, the suspension was centrifuged and three aliquots of the supernatant solution were titrated with a standardized solution of NaOH (2×10^{-3} M). The N% was calculated as the average value over the three independent titrations.



Scheme 1. Exohedrally N-decorated MWCNTs (MW@N₁₋₆) as metal free-catalysts for the CO₂ reduction reaction (CO₂RR).

2.1. Electrochemical Measurements

2.1.1. Working Electrode Preparation

A catalyst ink was prepared by dispersing 30 mg of each MW@N₁₋₆ sample in 2.5 g of isopropanol, 1.5 g of pure Milli-Q[®] water and 70 mg of a 5 wt.% Nafion solution in lower aliphatic alcohols and water. The resulting suspension was then sonicated for 60 min until a homogeneous ink was obtained. The latter was then deposited on carbon cloth (12–16 cm², cleaned, dried and weighted before deposition) by brush painting through seven–nine successive deposition/drying cycles. Teflonized Carbon cloth (Graphitstore[®], 410 μm thickness) was cleaned before use by sonication in a 1:1 water:isopropanol solution and finally dried at 70 °C to constant weight. The catalyst loading on the as-prepared electrode was determined by weight difference between the cathode and the bare carbon cloth and fixed to 1.2 ± 0.1 mg/cm² for each sample.

2.1.2. Cell Assembly

Electrochemical measurements were conducted in a home-made vertically oriented three-dimensionally (3D)-printed ABS [45] cell designed with a gas collector on the top (Figure S1) and divided into two halves hosting the cathodic and anodic compartments separated by a Nafion[®] 117 membrane. The cathode (working electrode) was secured by a screw-terminal connected to an insulated copper wire. The Ag/AgCl/KCl_{sat} reference electrode was placed in close proximity to the working electrode while a Pt wire, employed as counter-electrode, was set in the anodic part. Both compartments were filled with a 0.1 M KHCO₃ solution and sealed with rubber gaslock[®] plugs. Prior

to each measurement, the cathodic part was saturated by bubbling CO₂ (99.99% purity) for 30 min and the collector cone gas headspace was completely evacuated and filled with the electrolyte.

2.1.3. Electrolysis Experiments and Products Analysis

The electrolysis experiments were conducted at different potential values (ranging from -1.0 to -1.5 V vs. Ag|AgCl|KCl_{sat.}) at electrolysis times ranging from 10 min to 3 h depending on the applied potential and resulting currents. After each electrolysis run, 100 μ L of gases collected within the cone were withdrawn using a Hamilton gastight syringe and analyzed by gas chromatography (Carboxen Column, settled up with a heating ramp designed to separate H₂, O₂, N₂, CO, CO₂ and C₁–C₃ gases). The cell was then saturated again with CO₂ and the experiment repeated changing the applied potential. The cathodic liquid was collected at the end of each experimental cycle and analyzed by HPLC chromatography in order to detect any trace of liquid reduction products. Measurements were run on a Shimadzu-UFLC apparatus under isothermal conditions (65 °C), equipped with a refractive index detector (RID) and an Alltech OA-1000 Organic Acid Column of 300 mm (length) and 6.5 mm (i.d.). A 0.01 N H₂SO₄ solution was used as eluent at a flow rate of 0.4 mL min⁻¹. The KHCO₃ buffer solution is suppressed by passing the sample in cation exchange resin, prior to the injection. The same procedure was performed for the standard HCOOH solutions. The Faradaic efficiency (FE%) of the products were calculated from GC analysis data and CO productivities (expressed as NL^{CO} g_N⁻¹ h⁻¹) at fixed potential values have been calculated according to the relative current density values.

2.2. Computational Methods

The structures of surface N-containing groups (as zero-charge, H-saturated heterocycles) at the CNTs were optimized with a B3LYP functional [46] using a 6–31G** basis set on all atoms. A Grimme D3 dispersion correction was also included in the optimization, through the Gaussian IOp(3/124 = 30) keyword [47]. Bader charge partitioning was made through the free algorithm developed at Texas University available at <http://theory.cm.utexas.edu/bader/>. The Gaussian *.cube file from the optimizations was taken as the starting point for the Bader analysis on a charge density grid [48].

3. Results and Discussion

The study sheds light on the role played by carbon atoms neighboring N-sites of variably substituted pyridine nuclei, employed as metal-free active sites for CO₂RR. To this aim, five N-decorated multi-walled carbon nanotubes containing variably substituted pyridine nuclei together with a model N-pyrrolic functionalized sample have been prepared according to literature procedures (Scheme 1, MW@N₁ [40,41]; MW@N₂ [37,41]; MW@N₃ [43]; MW@N₄ [43]; MW@N₅ and MW@N₆ [41]). We took advantage of well consolidated aryldiazonium salt functionalization protocols as efficient synthetic tools for the exohedral covalent grafting of MWCNTs with pyridine- and pyrrole-containing dangling moieties (Scheme 1). All N-decorated samples have been thoroughly characterized in terms of N-content (elemental analysis and acid-base titration) and N-configuration of dangling heterocycles available at the outer material surface (XPS) before being fabricated into carbon cloth (Cc) electrodes (see details provided in the Experimental Section) and tested as metal-free systems for CO₂RR under comparable conditions (*vide infra*).

Sample MW@N₆ containing carbazole units was prepared as a model of a non-basic N-containing heterocycle embedded in a conjugated sp² framework similar to MW@N₂. Although the role of N-configuration of heterodopants (N-pyridinic, N-pyrrolic, N-aminic and N-quaternary) in complex carbon nanomaterials remains controversial, it is accepted that inclusion of nitrogen(s) contributes to break the electroneutrality of Csp² networks and generates carbon sites proximal to the heteroelement that take part (somehow) to CO₂ activation and its subsequent electrochemical reduction. There is an interesting parallelism between the supposed mechanism at work in N-doped nanocarbons applied to CO₂RR and their action as metal-free electrocatalysts within another highly challenging electroreduction process: the oxygen reduction reaction (ORR) [49,50]. MW@N₁ and MW@N₂ were previously reported

by us as benchmark metal-free ORR electrocatalysts containing well defined edge-type N-defects exposed in carbon nanostructures as effective sites for the process to occur [41,43]. Similar to ORR, a redistribution of the charge density around the nitrogen atoms in these metal-free systems creates high-energy carbon sites (typically proximal to the heteroelement) that improve the material adsorption properties towards CO₂ or its reduction intermediates, hence facilitating its overall electrochemical conversion [31,44]. The electronic charge distribution on the selected N-heterocycles can be invoked as a descriptor for the catalyst/substrate interaction once a methodology for the fine tuning of N-dopants in C-nanostructures is properly set-up. In addition, N-basic heterocycles (with pyridinic basicity > pyrrolic basicity) naturally foster the interaction of the metal-free electrocatalyst with acidic molecules (i.e., CO₂) thus favoring the generation of local gradients of CO₂ concentration close to the catalyst active sites. Our approach to the covalent grafting of tailored N-containing functionalities at the surface of C-based nanomaterials allows to play on the electronic properties of the heterocycles through an *ad-hoc* selection of electron donating (ED) or electron withdrawing (EW) groups attached to the rings. By this way, a fine tuning of the electronic charge density distribution at the N-site as well as at its neighboring carbon atoms [22] can be achieved for each dangling functional group (N₁-N₆).

All prepared N-decorated samples have been fully characterized by different techniques before being handled to prepare the corresponding electrodes for CO₂RR (see experimental section). To this aim, X-ray photoelectron spectroscopy (XPS), elemental analysis and acid-base titration (whenever applicable) were accomplished and data are outlined in Figure 1 and Table 1.

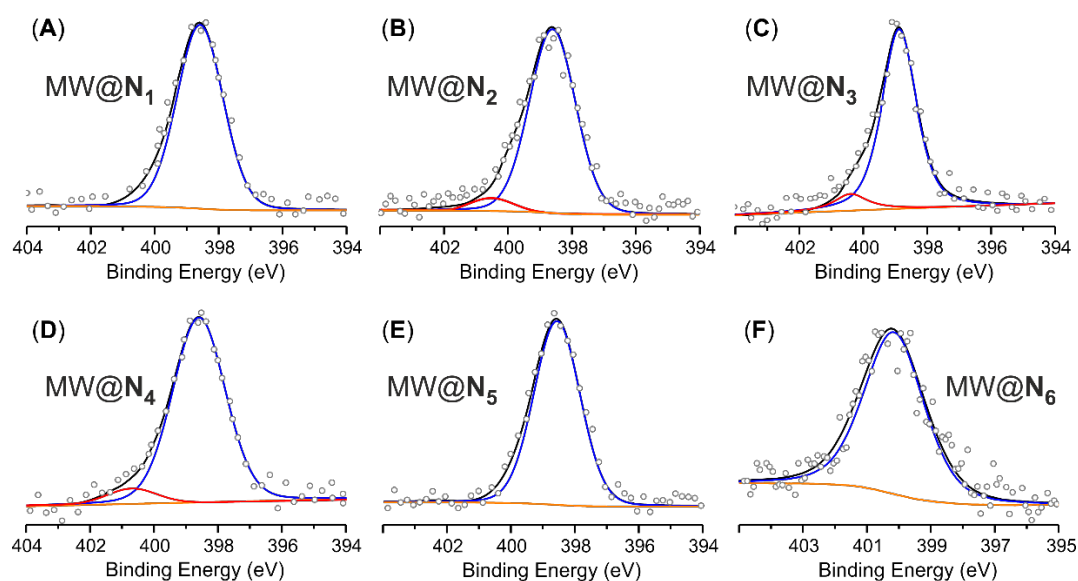


Figure 1. High resolution X-ray photoelectron spectroscopy (XPS) N 1s core level regions for samples MW@N₁ (A); MW@N₂ (B); MW@N₃ (C); MW@N₄ (D); MW@N₅ (E); MW@N₆ (F) along with their respective peak fittings.

Table 1. Calculation of the N-loading on each functionalized sample MW@N₁₋₆.

Samples	Elemental Analysis ^a		N (wt.%) ^c [mmol g ⁻¹] ^d	Acid-base titration ^b N _{Py} (wt.%) [mmol g ⁻¹] ^d	XPS analysis N (at.%) [mmol g ⁻¹] ^f
	C (%)	N (%)			
MWCNTs ^e	94.08	0.20	1.56; [1.11]	1.42; [1.01]	2.0; [1.01]
MW@N ₁	90.18	1.76			
MWCNTs ^{e,g}	92.34	0.29	1.28; [0.91]	1.27; [0.91]	1.6; [1.33]
MW@N ₂	91.35	1.57			

Table 1. Cont.

Samples	Elemental Analysis ^a			Acid-base titration ^b	XPS analysis
	C (%)	N (%)	N (wt.%) ^c [mmol g ⁻¹] ^d	N _{Py} (wt.%) [mmol g ⁻¹] ^d	N (at.%) [mmol g ⁻¹] ^f
MWCNTs ^e	94.56	0.07			
MW@N ₃	90.47	1.24	1.17; [0.84]	1.00; [0.71]	1.2; [1.00]
MWCNTs ^e	94.54	0.27			
MW@N ₄	91.35	2.14	1.87; [1.33]	1.63; [1.16]	2.0; [1.66]
MWCNTs ^e	93.67	0.09			
MW@N ₅	91.87	1.39	1.30; [0.93]	1.17; [0.84]	1.5; [1.24]
MWCNTs ^e	94.30	0.14			
MW@N ₆	90.89	2.83	2.69; [1.92]	-	2.9; [2.40]

^a Average C% and N% values calculated over three independent runs. ^b Average N% values calculated over three independent titration tests. ^c The N% content calculated as difference between the N-content (%) of each functionalized sample (MW@N₁₋₆) and the respective “blank sample” (MWCNTs). ^d Relative functional group loading. ^e “Blank samples” prepared using identical reaction conditions, reagents and work-up procedure applied to the synthesis of samples MW@N₁₋₆, except for the use of isopentyl nitrite as reagent. ^f Relative functional group loading calculated from the extrapolated N (wt.%). ^g Used in CO₂RR (see Figure 2A,B).

Figure 1A–E show typical N 1s profiles for samples MW@N₁₋₅ featured by a unique component in the 398.8–398.6 eV range, consistent with the presence of pyridine-type nuclei [51]. One component at higher binding energy values (400.3 eV) was measured in MW@N₆ (Figure 1F) in accordance with the presence of N-pyrrolic heterocycles [52]. Finally, minor N 1s shoulders at higher binding energy values and present in selected samples from this series (Figure 1B–D) were attributed to commonly observed and not-catalytically relevant nanomaterial contaminations [41,42,53,54] raising from solvents and/or reagents residues retained by the material porosity and not entirely removed throughout the work-up procedure.

Previous studies have confirmed that pristine MWCNTs as such did not show any CO₂ electroreduction performance, with HER being the only electrocatalytic process at work under more reducing overpotentials [37]. On the other hand, qualitative cyclic voltammetric (CV) tests conducted under N₂ and CO₂ saturated conditions with functionalized MWCNTs containing dangling N-groups at their outer surface resulted into electroactive catalysts featuring with variable CO₂ conversion/reduction properties depending on the nature of the N-containing group engaged in the electroreduction process [20,37]. Accordingly, all new electrocatalytic materials prepared in this contribution (MW@N₁₋₆) and MWCNTs were fabricated into carbon cloth (Cc) working electrodes (MW@N₁₋₆/Cc and MWCNTs/Cc) and directly scrutinized as CO₂RR electrocatalysts within a home-made 3D-printed ABS [45] three-electrode cell operating in a 0.1 M KHCO₃ solution, equipped with an Ag|AgCl|KCl_{sat} reference electrode, a Pt counter electrode in the anodic compartment separated by a Nafion[®] 117 membrane and a gas collector cone on the top for the regular sampling of all produced volatiles (Figure S1). All gaseous products (H₂ and CO only) generated throughout the electrocatalytic runs conducted at variable potentials have been systematically sampled using a gas-tight syringe and injected in a gas chromatograph (GC) for analysis. Finally, the possible formation of liquid reduction products has been verified through HPLC analysis of all solutions collected at the end of each electrochemical run.

One main advantage of our metal-free catalyst technology is the given possibility to rule out any contribution to CO₂ electrocatalytic reduction raising from the presence of metal impurities potentially present in pristine carbon nanomaterials (MWCNTs). Indeed, it has been well recognized that such ubiquitous impurities (often catalytically active in electrocatalysis) cannot be completely removed from classically prepared N-doped nanocarbons even after thorough purification procedures [55]. Our approach to electrocatalysts preparation allows to test pristine MWCNTs as a blank sample

in the process (*vide infra*). Accordingly, their comparison with *ad-hoc* N-functionalized materials unambiguously explains the role played by *exohedral* N-groups only in CO₂RR.

The total current density values and composition of reaction products have been determined for each electrocatalyst in the $-1.0 \div -1.5$ V range at electrolysis time lengths varying from 10 min to 3 h as a function of the applied potential. Longer electrolysis times at lower overpotentials have been applied in order to collect a reasonable amount of gas for an accurate GC analysis of products and their relative ratio. Irrespective of the electrocatalyst at work, only gaseous products have been detected with MW@N₁₋₆, with CO being the unique component from CO₂ electroreduction along with H₂ as a side-product from water electrolysis (HER). No sample from this series led to the formation of liquid products, whatever the electroreduction potential applied to the cell. According to our previous evidences with pristine MWCNTs, only H₂ was detected after electrolysis with MWCNT/Cc even under CO₂ saturated atmosphere [37]. As mentioned above, this blank trial confirmed the role played by exohedral and discrete N-functionalities in MW@N₁₋₆ in CO₂RR and it rules out any potential contribution raising from the metallic residues in C-nanocarriers.

Figure 2A summarizes the CO faradaic efficiency (FE_{CO}) values measured on each N-decorated electrocatalyst as a function of the applied potential, while Figure 2B refers to the CO current density (J_{CO}) values given for each electrocatalyst (MW@N₁₋₆/Cc) at -1.1 V. The latter potential was selected as the mean V value in the range where all electrocatalysts offer their highest FE_{CO} (J_{tot} values registered at V where each electrocatalyst shows its highest FE_{CO} are outlined on Figure S2 for the sake of completeness). Figure S3 reports the H₂ faradaic efficiency (FE_{H2}) plots for MW@N₁₋₆/Cc in the $-1.0 \div -1.5$ V range, while Table S1 details J_{CO} and J_{tot} values given for each electrocatalyst at -1.1 V along with productivity values calculated for each MW@N₁₋₆/Cc electrocatalyst and expressed as $NL^{CO} g_N^{-1} h^{-1}$.

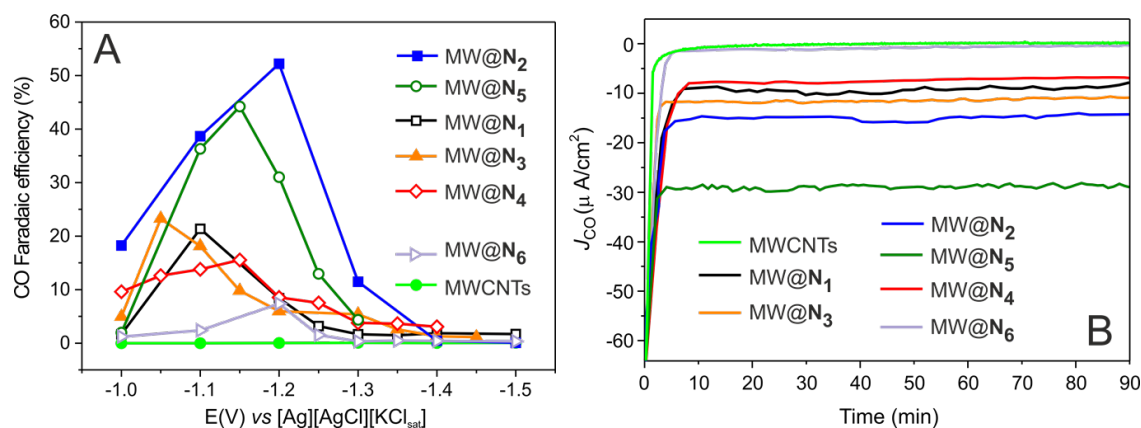


Figure 2. CO₂ Electroreduction performance with MW@N₁₋₆ and MWCNTs fabricated as carbon cloth-based electrodes and used in 0.1 M KHCO₃ solution as electrolyte. (A) CO faradaic efficiency as a function of the applied potentials. (B) CO current density values (J_{CO}) and their stability vs. time, measured for each electrocatalytic material MW@N₁₋₆ at -1.1 V as potential.

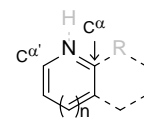
As a first trial, pristine MWCNTs were fabricated into a Cc electrode and tested as a pure carbon-based electrocatalyst (blank sample) for the process. As Figure 2A and Table S1 show, MWCNTs revealed null or negligible activity in CO₂RR whatever the applied potential in the $-1.0 \div -1.5$ V range vs. reference electrode. On the other hand, the acridine and 2,6(Me)₂Py-functionalized electrocatalysts MW@N₂/Cc and MW@N₅/Cc were the most performing CO₂RR systems from this series, showing FE_{CO} values up to 52 and 44% at -1.2 V and -1.15 V vs. Ag|AgCl|KCl_{sat}, respectively (Figure 2A and Table S1, entries 7 and 16). Notably, the plain Pyridine-functionalized electrocatalyst (MW@N₁) showed only moderate CO₂RR performance with an FE_{CO} of 21% at -1.1 V vs. the reference electrode. As expected, at more reducing potentials (up to -1.5 V), HER was the main side-process at work

with all these metal-free electrocatalysts (Table S1, entries 4, 7, 16 vs. 5, 8, 17, and Figure S3). In spite of an identical N-configuration for the three heterocycles (only N-pyridinic sites in MW@N₂, MW@N₅ and MW@N₁) and a very close N-loading of dangling groups in each sample (Table 1), their different electrocatalytic behavior prompted us to postulate the existence of a key-action played by the electronic charge distribution in each N-pyridinic heterocycle. Such an electronic distribution, driven by the nature and position of ring-substituents, was supposed to modulate the inherent ability of N-containing groups to interact more or less efficiently with CO₂ and/or its reduction intermediates. To this aim, the *o*-methoxy pyridine (MW@N₃) and naphthyridine-functionalized (MW@N₄) samples were fabricated into Cc electrodes and studied as CO₂RR electrocatalysts under identical conditions. Once again, both samples showed only moderate performance with FE_{CO} as high as 23% and 15% at −1.05 V and −1.15 V vs. [Ag][AgCl][KCl_{sat}] for MW@N₃/Cc and MW@N₄/Cc, respectively (Figure 2A and Table S1, entries 9 and 13). As an additional trial, carbazole-functionalized MWCNTs (N-pyrrolic heterocycle) were scrutinized as CO₂RR electrocatalysts in the same potential range. As Figure 2 clearly shows, MW@N₆/Cc was the worst electrocatalyst for the process with a maximum of 7% FE_{CO} at −1.20 V vs. [Ag][AgCl][KCl_{sat}], irrespective to its relatively high N-loading [56].

Figure 2B finally refers to J_{CO} values vs. time as measured for each electrocatalyst at −1.1 V as potential (see also Table S1). Current densities (mA/cm²) are constant throughout the whole electrochemical runs thus confirming the excellent stability of each functionalized material (produced in the form of Cc electrocatalyst), under CO₂RR conditions. In addition, the XPS N 1s core region profile of the most representative sample from this series (MW@N₂) recorded on the recovered electrocatalyst (after 90 min CO₂RR) did not show any qualitative profile alterations (Figure S4).

This comparative study among tailored N-decorated carbon-based electrocatalysts suggests the existence of coherent descriptors for the CO faradaic efficiency (FE_{CO}): the N-configuration (N-pyridinic vs. N-pyrrolic) of the exohedral dopant(s) and the electronic charge density distribution at the N-neighboring carbon atoms of each dangling heterocycle. To better rationalize this descriptor, we have carried out a DFT pre-optimization on each dangling substituent (N₁–N₆) at the B3LYP//6–31G** level of theory and a Bader charge analysis has been performed to deduce the Bader atomic charges present on both N and C_α atoms, whose values are outlined in Table 2. In general, the numerical values obtained through our calculations are comparable to those appearing in other literature studies performed on similar metal-free hetero-doped carbon nanomaterials [57–59]; this makes us confident about the accuracy of our calculations. The N atomic charge measured on each heterocycle is roughly the same on all N-pyridinic nuclei (N_{1–5}), with minor differences ascribable to the delocalization of the nitrogen electronic lone pair as a function of the ring substituents. Such electronic charge values are a measure of the Lewis-basic properties of N-sites in N_{1–5}, and hence, a measure of the interaction strength with a Lewis-acid reagent such as CO₂. The higher the electronic charge density at the N-site, the higher the affinity towards CO₂. As a matter of fact, the poorly basic carbazole N₆ (featuring a lower N electronic charge density) will show a reduced affinity for CO₂. Such an acid-base interaction is supposed to be at the origin of the electrocatalytic activity of pyridine-based metal-free electrocatalysts and it reduces the free energy barriers associated to the first (and kinetically sluggish) electron transfer process [60]. A more pronounced difference in qC_{α} values measured on all variably substituted heterocycles prompted us to look for a coherent correlation between qC_{α} and the different process selectivity towards CO (FE_{CO}) measured on each electrocatalyst. Indeed, absorption and stabilization of CO₂ and its reduction intermediates at the carbon atoms adjacent to N sites are also claimed as a key driving force for the process to occur [31,44]. Figure 3 was obtained by plotting the FE_{CO} value recorded on each N-decorated sample (MW@N_{1–6}) at −1.1 V vs. the qC_{α} value calculated at the respective heterocycles. A mean qC value between C_α and C_{α'} was arbitrarily considered for both dissymmetrical N₃ and N₄ samples without altering the general trend outlined in Figure 3.

Table 2. Net Bader charges (q) calculated at N and C_α atoms on N_{1-6} heterocycles. Bader analysis of the atomic charge density on previously reported N_{1-2} and N_6 systems [41] has also been listed here for completeness.

Entry	N-heter.	n	q_N		
				q_{C_α}	$q_{C_{\alpha'}}$
1	N_1	1	-2.670	1.161	1.161
2	N_2	1	-2.696	1.448	1.448
3	N_3	1	-2.845	2.467	1.208
4	N_4	1	-2.745	2.649	1.293
5	N_5	1	-2.760	1.291	1.291
6	N_6	0	-2.356	0.828	0.828

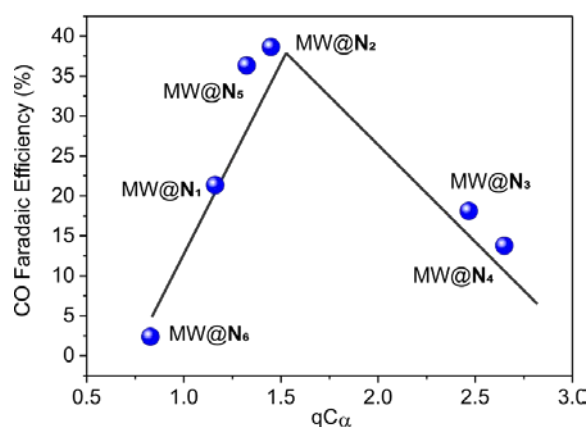
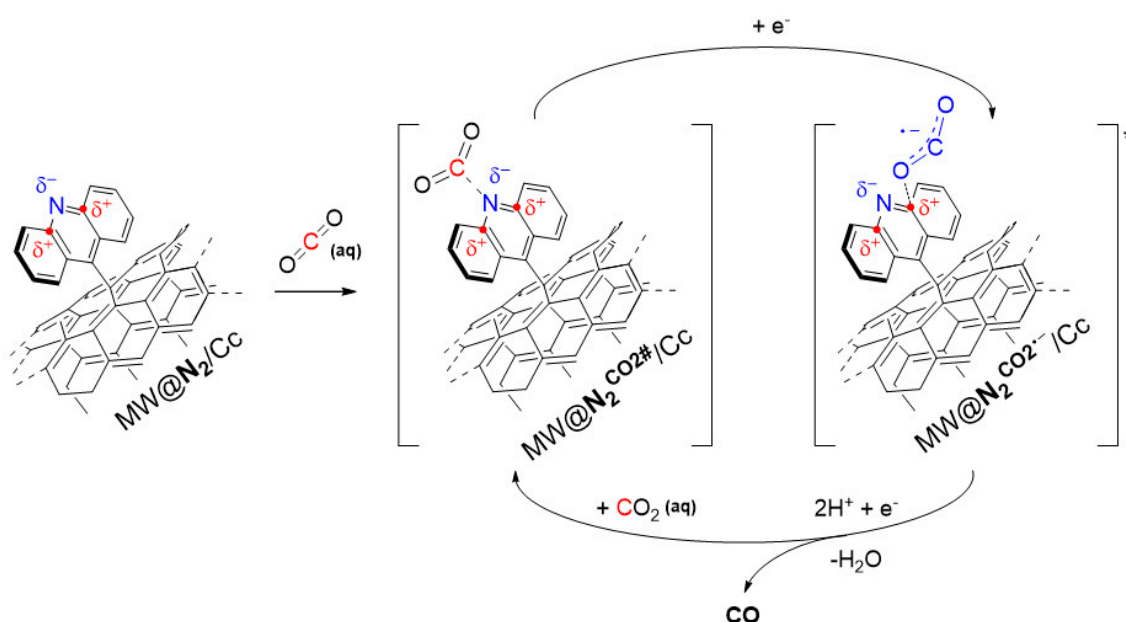


Figure 3. Volcano plot for CO_2RR on N-decorated samples $MW@N_{1-6}$. FE_{CO} was measured for each electrocatalyst at -1.1 V.

At first glance, data on Figure 3 follow a typical volcano plot with the acridine-decorated $MW@N_2$ sample being the best performing CO_2RR system among the scrutinized materials. It can be inferred that both the basic character of the N-containing heterocycles and the electronic charge distribution at $C_\alpha/C_{\alpha'}$ play a role on the ultimate electrocatalytic performance of these metal-free systems. While the former is expected to foster CO_2 interaction with N-dangling groups (reducing the energy barriers for the first electron transfer), the latter is expected to stabilize (more or less efficiently) the resulting radical anion $CO_2^{\bullet-}$ before its further reduction to CO [23] (see Scheme 2 for an hypothetical CO_2 and $CO_2^{\bullet-}$ interaction mode on acridine decorated MWCNTs as a model N-decorated/Cc example). The lower the q_{C_α} value (N_1 and N_6), the weaker the stabilization of the radical anion $CO_2^{\bullet-}$ and the driving-force to its generation. On the other hand, the higher the positive C_α charge, the strongest the resulting $CO_2^{\bullet-}$ stabilization that hurdles its further reduction to CO. Because of relatively low (N_1 and N_6) or relatively high (N_3 and N_4) $CO_2^{\bullet-}$ adsorption energies at C_α , hydrogen evolution largely dominates over CO_2 reduction with these electrocatalysts.

2,6-(Me)₂Py and acridine frameworks (in $MW@N_5$ and $MW@N_2$, respectively) create an ideal balance between N-basicity for CO_2 activation/conversion to give the corresponding $CO_2^{\bullet-}$ radical ion (first e^- transfer) and its subsequent stabilization by neighboring C-sites.



Scheme 2. CO₂ electroreduction process on model N-acridine decorated MWCNTs (MW@N₂/Cc) via CO₂(aq) adsorption/activation (CO₂[#]) at the basic pyridinic nitrogen followed by a first 1e⁻ reduction step to give the CO₂^{•*} radical ion stabilized (*) at C_α/C_{α'} of the heterocycle. A further 1e⁻ reduction produces (CO + H₂O) and regenerates CO₂[#] that closes the catalytic cycle.

These conclusions are in line with evidences by Su et al. based on density functional theory (DFT) calculations carried out on N-doped carbon nanotubes containing variable fractions of pyrrolic, pyridinic and quaternary N-species. These authors demonstrated that improved activity of doped nanocarbons as electrocatalysts for CO₂RR can be achieved via stabilization of the key intermediate CO₂^{•*} [28]. The same authors also pointed out that another important factor that influences the selectivity of N-doped carbon materials in the CO₂-to-CO conversion is the ability to release the reaction product CO at the end of the catalytic cycle. The different thermodynamic affinity for carbon monoxide has been estimated through the calculation of the corresponding Gibbs energy values (ΔG) of the adduct formation (CO + N-heterocycle \rightarrow adduct). The results showed that pyridinic N-sites are featured by a very low interaction strength with CO compared to other N-configurations. This finding is fully consistent with our experimental evidences, where even for the most performing electrocatalyst from this series (MW@N₂), CO was the unique reduction product detected both in gas and liquid-phase.

4. Conclusions

This contribution describes a series of exohedrally N-decorated carbon nanomaterials with variably substituted N-pyridine nuclei as model metal-free electrocatalysts for the selective CO₂-to-CO electroreduction. The functionalization approach, used to introduce tailored N-functionalities at the nanomaterial surface of electrically conductive C-nanocarriers, offers a useful tool to shed light on the role played by these heterocycles in CO₂RR. It allows to finely tune the electronic properties of all covalently linked heterocycles, with a consequent control of the electronic charge density distribution at the N-site and its neighboring C_α/C_{α'} atoms. A comparative CO₂RR electrochemical screening of all N-decorated samples has suggested the existence of a coherent descriptor (a volcano-like trend) between the catalyst's CO faradaic efficiency (FE_{CO}) and the electronic charge density distribution on each heterocycle engaged in the process. It can be inferred that both the basic character of each heterocycle as well as the electronic charge distribution at C_α/C_{α'} play a role on the ultimate electrocatalytic performance of these metal-free systems. While the former is supposed to foster CO₂ interaction with

N-dangling groups (reducing the energy barriers for the first electron transfer), the latter is expected to stabilize the resulting radical anion $\text{CO}_2^{\bullet-}$ before its further reduction to CO. Accordingly, the ideal balance between N-heterocycle basicity and $\text{CO}_2^{\bullet-}$ radical ion stabilization ability by neighboring C-sites is at the origin of the catalyst selectivity towards CO (FE_{CO}).

These findings allow to shed light on the role of pyridinic nuclei in CO_2 RR by N-doped nanocarbons; they provide a privileged viewpoint on the reaction mechanism at work and they offer a useful tool for the preparation of more catalytically active systems for the process.

Supplementary Materials: The following are available online at <http://www.mdpi.com/1996-1073/13/11/2703/s1>, Figure S1: Scheme of the home-made 3D-printed ABS three-electrode cell used in the study; Figure S2: Total current density values (J_{tot}) and their stability vs. time, measured for each electrocatalytic material MW@N_{1-6} at the potential value where they present the highest FE_{CO} ; Figure S3: H_2 faradaic efficiency as a function of the applied potential ($-1.0 \div -1.5$ V range); Figure S4: N 1s core regions and relative fits for the high resolution XPS spectrum of MW@N_2 before (A) and after (B) CO_2 RR. Sample B has been recovered from $\text{MW@N}_2/\text{Cc}$ after 90 min of electrocatalytic run; Table S1: J_{tot} , J_{CO} , CO and H_2 faradaic efficiency (FE) and productivity obtained with $\text{MW@N}_{1-6}/\text{Cc}$ and MWCNT/Cc .

Author Contributions: Conceptualization, F.V. and G.G.; Data curation, A.R., L.L., C.P.-H., F.V. and G.G.; Formal analysis, G.T., J.F., A.R., L.L. and D.Y.; Funding acquisition, F.V. and G.G.; Investigation, G.T., J.F., D.Y. and G.G.; Methodology, A.R., L.L. and G.G.; Resources, G.G.; Validation, G.T. and C.P.-H.; Writing—original draft, G.G.; Writing—review and editing, F.V. All authors have read and agreed to the published version of the manuscript.

Funding: This research was funded by the TRAINER project (Catalysts for Transition to Renewable Energy Future) of the “Make our Planet Great Again” program (Ref. ANR-17-MPGA-0017), by the Italian MIUR through the PRIN 2017 Projects Multi-e (20179337R7) “Multielectron transfer for the conversion of small molecules: an enabling technology for the chemical use of renewable energy” and (2017YH9MRK) “Novel Multilayered and Micro-Machined Electrode Nano-Architectures for Electrocatalytic Applications (Fuel Cells and Electrolyzers) by the Ente Cassa di Risparmio di Firenze through the “EnergyLab” project.

Acknowledgments: This work is performed according to the Russian Government Program of Competitive Growth of Kazan Federal University.

Conflicts of Interest: The authors declare no competing interests.

References

1. Martens, J.A.; Bogaerts, A.; De Kimpe, N.; Jacobs, P.A.; Marin, G.B.; Rabaey, K.; Saeys, M.; Verhelst, S. The Chemical Route to a Carbon Dioxide Neutral World. *ChemSusChem* **2010**, *10*, 1039–1055. [[CrossRef](#)] [[PubMed](#)]
2. Roy, S.; Cherevotan, A.; Peter, S.C. Thermochemical CO_2 Hydrogenation to Single Carbon Products: Scientific and Technological Challenges. *ACS Energy Lett.* **2018**, *3*, 1938–1966. [[CrossRef](#)]
3. Appel, A.M.; Bercaw, J.E.; Bocarsly, A.B.; Dobbek, H.; DuBois, D.L.; Dupuis, M.; Ferry, J.G.; Fujita, E.; Hille, R.; Kenis, P.J.A.; et al. Frontiers, Opportunities, and Challenges in Biochemical and Chemical Catalysis of CO_2 Fixation. *Chem. Rev.* **2013**, *113*, 6621–6658. [[CrossRef](#)] [[PubMed](#)]
4. Lu, Q.; Jiao, F. Electrochemical CO_2 reduction: Electrocatalyst, reaction mechanism, and process engineering. *Nano Energy* **2016**, *29*, 439–456. [[CrossRef](#)]
5. Mohammadi, A.; Mehrpooya, M. A comprehensive review on coupling different types of electrolyzer to renewable energy sources. *Energy* **2018**, *158*, 632–655. [[CrossRef](#)]
6. Hori, Y. *Modern Aspects of Electrochemistry*; Vayenas, G.C., White, E.R., Eds.; Springer: Patras, Greece, 2008; p. 89.
7. Kortlever, R.; Shen, J.; Schouten, K.J.P.; Calle-Vallejo, F.; Koper, M.T.M. Catalysts and Reaction Pathways for the Electrochemical Reduction of Carbon Dioxide. *J. Phys. Chem. Lett.* **2015**, *6*, 4073–4082. [[CrossRef](#)]
8. Kuhl, K.P.; Cave, E.R.; Abram, D.N.; Jaramillo, T.F. New insights into the electrochemical reduction of carbon dioxide on metallic copper surfaces. *Energy Environ. Sci.* **2012**, *5*, 7050–7059. [[CrossRef](#)]
9. Zheng, T.; Jiang, K.; Wang, H. Recent advances in electrochemical CO_2 -to-CO conversion on heterogeneous catalysts. *Adv. Mater.* **2018**, *30*, 1802066. [[CrossRef](#)]
10. Khodakov, A.Y.; Chu, W.; Fongarland, P. Advances in the Development of Novel Cobalt Fischer–Tropsch Catalysts for Synthesis of Long-Chain Hydrocarbons and Clean Fuels. *Chem. Rev.* **2007**, *107*, 1692–1744. [[CrossRef](#)]

11. Centi, G.; Perathoner, S. Opportunities and Prospects in the Chemical Recycling of Carbon Dioxide to Fuels. *Catal. Today* **2009**, *148*, 191–205. [[CrossRef](#)]
12. Jiang, K.; Siahrostami, S.; Akey, A.J.; Li, Y.; Lu, Z.; Lattimer, J.; Hu, Y.; Stokes, C.; Gangishetty, M.; Chen, G.; et al. Transition-Metal Single Atoms in a Graphene Shell as Active Centers for Highly Efficient Artificial Photosynthesis. *Chem* **2017**, *3*, 950–960. [[CrossRef](#)]
13. Feng, D.-M.; Zhu, Y.-P.; Chen, P.; Ma, T.-Y. Recent advances in transition-metal-mediated electrocatalytic CO₂ reduction: From homogeneous to heterogeneous systems. *Catalysts* **2017**, *7*, 373. [[CrossRef](#)]
14. Francke, R.; Schille, B.; Roemelt, M. Homogeneously Catalyzed Electroreduction of Carbon Dioxide-Methods, Mechanisms, and Catalysts. *Chem. Rev.* **2018**, *118*, 4631–4701. [[CrossRef](#)] [[PubMed](#)]
15. Yang, Y.; Ajmal, S.; Zheng, X.; Zhang, L. Efficient nanomaterials for harvesting clean fuels from electrochemical and photoelectrochemical CO₂ reduction. *Sustain. Energy Fuels* **2018**, *2*, 510–537. [[CrossRef](#)]
16. Zhang, L.; Zhao, Z.-J.; Gong, J. Nanostructured materials for heterogeneous electrocatalytic CO₂ reduction and their related reaction mechanisms. *Angew. Chem. Int. Ed.* **2017**, *56*, 11326–11353. [[CrossRef](#)]
17. Zhang, W.; Hu, Y.; Ma, L.; Zhu, G.; Wang, Y.; Xue, X.; Chen, R.; Yang, S.; Jin, Z. Progress and perspective of electrocatalytic CO₂ reduction for renewable carbonaceous fuels and chemicals. *Adv. Sci.* **2018**, *5*, 1700275. [[CrossRef](#)]
18. Bevilacqua, M.; Filippi, J.; Miller, H.A.; Vizza, F. Recent technological progress in CO₂ electroreduction to fuels and energy carriers in aqueous environments. *Energy Technol.* **2015**, *3*, 197–210. [[CrossRef](#)]
19. Sharma, P.P.; Wu, J.; Yadav, R.M.; Liu, M.; Wright, C.J.; Tiwary, C.S.; Yakobson, B.I.; Lou, J.; Ajayan, P.M.; Zhou, X.-D. Nitrogen-doped carbon nanotube arrays for high-efficiency electrochemical reduction of CO₂: On the understanding of defects, defect density, and selectivity. *Angew. Chem. Int. Ed.* **2015**, *54*, 13701–13705. [[CrossRef](#)]
20. Duan, X.; Xu, J.; Wei, Z.; Ma, J.; Guo, S.; Wang, S.; Liu, H.; Dou, S. Metal-Free Carbon Materials for CO₂ Electrochemical Reduction. *Adv. Mater.* **2017**, *29*, 1701784. [[CrossRef](#)]
21. Chai, G.-L.; Guo, Z.-X. Highly effective sites and selectivity of nitrogendoped graphene/CNT catalysts for CO₂ electrochemical reduction. *Chem. Sci.* **2016**, *7*, 1268–1275. [[CrossRef](#)]
22. Kumar, B.; Asadi, M.; Pisasale, D.; Sinha-Ray, S.; Rosen, B.A.; Haasch, R.; Abiade, J.; Yarin, A.L.; Salehi-Khojin, A. Renewable and metal-free carbon nanofibre catalysts for carbon dioxide reduction. *Nat. Commun.* **2013**, *4*, 2819. [[CrossRef](#)]
23. Li, W.; Seredych, M.; Rodriguez-Castellon, E.; Bandoz, T.J. Metal-free nanoporous carbon as a catalyst for electrochemical reduction of CO₂ to CO and CH₄. *ChemSusChem* **2016**, *9*, 606–616. [[CrossRef](#)] [[PubMed](#)]
24. Lu, X.; Tan, T.H.; Ng, Y.H.; Amal, R. Highly selective and stable reduction of CO₂ to CO by a graphitic carbon nitride/carbon nanotube composite electrocatalyst. *Chem. Eur. J.* **2016**, *22*, 11991–11996. [[CrossRef](#)]
25. Molly Jhong, H.-R.; Tornow, C.E.; Smid, B.; Gewirth, A.A.; Lyth, S.M.; Kenis, P.J.A. A nitrogen-doped carbon catalyst for electrochemical CO₂ conversion to CO with high selectivity and current density. *ChemSusChem* **2017**, *10*, 1094–1099. [[CrossRef](#)] [[PubMed](#)]
26. Wu, J.; Liu, M.; Sharma, P.P.; Yadav, R.M.; Ma, L.; Yang, Y.; Zou, X.; Zhou, X.-D.; Vajtai, R.; Yakobson, B.I.; et al. Incorporation of nitrogen defects for efficient reduction of CO₂ via two-electron pathway on three-dimensional graphene foam. *Nano Lett.* **2016**, *16*, 466–470. [[CrossRef](#)]
27. Wu, J.; Yadav, R.M.; Liu, M.; Sharma, P.P.; Sekhar Tiwary, C.; Ma, L.; Zou, X.; Zhou, X.-D.; Yakobson, B.I.; Lou, J.; et al. Achieving highly efficient, selective, and stable CO₂ reduction on nitrogen-doped carbon nanotubes. *ACS Nano* **2015**, *9*, 5364–5371. [[CrossRef](#)]
28. Xu, J.; Kan, Y.; Huang, R.; Zhang, B.; Wang, B.; Wu, K.-H.; Lin, Y.; Sun, X.; Li, Q.; Centi, G.; et al. Revealing the Origin of Activity in Nitrogen-Doped Nanocarbons towards Electrocatalytic Reduction of Carbon Dioxide. *ChemSusChem* **2016**, *9*, 1085–1089. [[CrossRef](#)]
29. Zhang, B.; Zhao, T.-J.; Feng, W.-J.; Liu, Y.-X.; Wang, H.-H.; Su, H.; Lv, L.-B.; Li, X.-H.; Chen, J.-S. Polarized few-layer g-C₃N₄ as metal-free electrocatalyst for highly efficient reduction of CO₂. *Nano Res.* **2018**, *11*, 2450–2459. [[CrossRef](#)]
30. Liu, Y.; Zhao, J.; Cai, Q. Pyrrolic-nitrogen doped graphene: A metal-free electrocatalyst with high efficiency and selectivity for the reduction of carbon dioxide to formic acid: A computational study. *Phys. Chem. Chem. Phys.* **2016**, *18*, 5491–5498. [[CrossRef](#)]

31. Wang, H.; Chen, Y.; Hou, X.; Ma, C.; Tan, T. Nitrogen-doped graphenes as efficient electrocatalysts for the selective reduction of carbon dioxide to formate in aqueous solution. *Green Chem.* **2016**, *18*, 3250–3256. [[CrossRef](#)]
32. Zhang, S.; Kang, P.; Ubnoske, S.; Brennaman, M.K.; Song, N.; House, R.L.; Glass, J.T.; Meyer, T.J. Polyethylenimine-enhanced electrocatalytic reduction of CO₂ to formate at nitrogen-doped carbon nanomaterials. *J. Am. Chem. Soc.* **2014**, *136*, 7845–7848. [[CrossRef](#)] [[PubMed](#)]
33. Liu, Y.; Chen, S.; Quan, X.; Yu, H. Efficient Electrochemical Reduction of Carbon Dioxide to Acetate on Nitrogen-Doped Nanodiamond. *J. Am. Chem. Soc.* **2015**, *137*, 11631–11636. [[CrossRef](#)] [[PubMed](#)]
34. Lum, Y.; Kwon, Y.; Lobaccaro, P.; Chen, L.; Clark, E.L.; Bell, A.T.; Ager, J.W. Trace levels of copper in carbon materials show significant electrochemical CO₂ reduction activity. *ACS Catal.* **2016**, *6*, 202–209. [[CrossRef](#)]
35. Siahrostami, S.; Jiang, K.; Karamad, M.; Chan, K.; Wang, H.; Nørskov, J. Theoretical investigations into defected graphene for electrochemical reduction of CO₂. *ACS Sustain. Chem. Eng.* **2017**, *5*, 11080–11085. [[CrossRef](#)]
36. Wu, J.; Ma, S.; Sun, J.; Gold, J.I.; Tiwary, C.S.; Kim, B.; Zhu, L.; Chopra, N.; Odeh, I.N.; Vajtai, R.; et al. A metal-free electrocatalyst for carbon dioxide reduction to multi-carbon hydrocarbons and oxygenates. *Nat. Commun.* **2016**, *7*, 13869. [[CrossRef](#)] [[PubMed](#)]
37. Tuci, G.; Filippi, J.; Ba, H.; Rossin, A.; Luconi, L.; Pham-Huu, C.; Vizza, F.; Giambastiani, G. How to Teach an Old Dog New (Electrochemical) Tricks: Aziridine-Functionalized CNTs as Efficient Electrocatalysts for the Selective CO₂ Reduction to CO. *J. Mater. Chem. A* **2018**, *6*, 16383–16389. [[CrossRef](#)]
38. Tuci, G.; Luconi, L.; Rossin, A.; Berretti, E.; Ba, H.; Innocenti, M.; Yakhvarov, D.; Caporali, S.; Pham-Huu, C.; Giambastiani, G. Aziridine-functionalized multiwalled carbon nanotubes: Robust and versatile catalysts for the oxygen reduction reaction and Knoevenagel condensation. *ACS Appl. Mater. Interfaces* **2016**, *8*, 30099–30106. [[CrossRef](#)]
39. Tuci, G.; Luconi, L.; Rossin, A.; Giambastiani, G. Chemical Functionalization of Carbon Nanomaterials: Bridging the Gap between Simple Carriers and Smart (Metalfree) Catalysts. *Chimia* **2017**, *71*, 568–572. [[CrossRef](#)]
40. Tuci, G.; Rossin, A.; Luconi, L.; Pham-Huu, C.; Cicchi, S.; Ba, H.; Giambastiani, G. Pyridine-decorated carbon nanotubes as a metal-free heterogeneous catalyst for mild CO₂ reduction to methanol with hydroboranes. *Catal. Sci. Technol.* **2017**, *7*, 5833–5837. [[CrossRef](#)]
41. Tuci, G.; Zafferoni, C.; D’Ambrosio, P.; Caporali, S.; Ceppatelli, M.; Rossin, A.; Tsoufis, T.; Innocenti, M.; Giambastiani, G. Tailoring Carbon Nanotube N-Dopants while Designing Metal-Free Electrocatalysts for the Oxygen Reduction Reaction in Alkaline Medium. *ACS Catal.* **2013**, *3*, 2108–2111. [[CrossRef](#)]
42. Tuci, G.; Zafferoni, C.; Rossin, A.; Luconi, L.; Milella, A.; Ceppatelli, M.; Innocenti, M.; Liu, Y.; Pham-Huu, C.; Giambastiani, G. Chemical functionalization of N-doped carbon nanotubes: A powerful approach to cast light on the electrochemical role of specific N-functionalities in the Oxygen Reduction Reaction. *Catal. Sci. Technol.* **2016**, *6*, 6226–6236. [[CrossRef](#)]
43. Tuci, G.; Zafferoni, C.; Rossin, A.; Milella, A.; Luconi, L.; Innocenti, M.; Truong Phuoc, L.; Duong-Viet, C.; Pham-Huu, C.; Giambastiani, G. Chemically functionalized carbon nanotubes with pyridine groups as easily tunable N-decorated nanomaterials for the oxygen reduction reaction in alkaline medium. *Chem. Mater.* **2014**, *26*, 3460–3470. [[CrossRef](#)]
44. Wang, H.; Jia, J.; Song, P.; Wang, Q.; Li, D.; Min, S.; Qian, C.; Wang, L.; Li, Y.F.; Ma, C.; et al. Efficient electrocatalytic reduction of CO₂ by nitrogen-doped nanoporous carbon/carbon nanotube membranes: A step towards the electrochemical CO₂ refinery. *Angew. Chem. Int. Ed.* **2017**, *56*, 7847–7852. [[CrossRef](#)]
45. ABS (Acrylonitrile-Butadiene-Styrene) is a common base-resistant thermoplastic polymer for 3D-printing.
46. Becke, A.D. Density-functional thermochemistry. III. The role of exact exchange. *J. Chem. Phys.* **1993**, *98*, 5648–5652. [[CrossRef](#)]
47. Grimme, S.A.J.; Ehrlich, S.; Krieg, H. A consistent and accurate ab initio parametrization of density functional dispersion correction (DFT-D) for the 94 elements H-Pu. *J. Chem. Phys.* **2010**, *132*, 154104. [[CrossRef](#)] [[PubMed](#)]
48. Tang, W.; Sanville, E.; Henkelman, G. A grid-based Bader analysis algorithm without lattice bias. *J. Phys. Condens. Matter* **2009**, *21*, 084204. [[CrossRef](#)]
49. Singh, S.K.; Takeyasu, K.; Nakamura, J. Active Sites and Mechanism of Oxygen Reduction Reaction Electrocatalysis on Nitrogen-Doped Carbon Materials. *Adv. Mater.* **2019**, *31*, 1804297. [[CrossRef](#)]

50. Dai, L.; Xue, Y.; Qu, L.; Choi, H.-J.; Baek, J.-B. Metal-Free Catalysts for Oxygen Reduction Reaction. *Chem. Rev.* **2015**, *115*, 4823–4892. [[CrossRef](#)]
51. Chizari, K.; Vena, A.; Laurentius, L.; Sundararaj, U. The effect of temperature on the morphology and chemical surface properties of nitrogen-doped carbon nanotubes. *Carbon* **2014**, *68*, 369–379. [[CrossRef](#)]
52. Louette, P.; Bodino, F.; Pireaux, J.-J. Poly(pyrrole) (PPY) XPS Reference Core Level and Energy Loss Spectra. *Surf. Sci. Spectra* **2005**, *12*, 84–89. [[CrossRef](#)]
53. Dyke, C.A.; Stewart, M.P.; Maya, F.; Tour, J.M. Diazonium-based functionalization of carbon nanotubes: XPS and GC-MS analysis and mechanistic implications. *Synlett* **2004**, *2004*, 155–160. [[CrossRef](#)]
54. Price, B.K.; Tour, J.M. Functionalization of Single-Walled Carbon Nanotubes “On Water”. *J. Am. Chem. Soc.* **2006**, *128*, 12899–12904. [[CrossRef](#)] [[PubMed](#)]
55. Wong, C.H.A.; Chua, C.K.; Khezri, B.; Webster, R.D.; Pumera, M. Graphene Oxide Nanoribbons from the Oxidative Opening of Carbon Nanotubes Retain Electrochemically Active Metallic Impurities. *Angew. Chem. Int. Ed.* **2013**, *52*, 8685–8688. [[CrossRef](#)]
56. The higher N-loading obtained for MW@N₆ is in line with the electron rich character of carbazole heterocycles and the consequent higher reactivity of their postulated aryl radical intermediates obtained during the Tour functionalization protocol.
57. Gouse Peera, S.; Sahu, A.K.; Arunchander, A.; Bhat, S.D.; Karthikeyan, J.; Murugan, P. Nitrogen and fluorine co-doped graphite nanofibers as high durable oxygen reduction catalyst in acidic media for polymer electrolyte fuel cells. *Carbon* **2015**, *93*, 130–142. [[CrossRef](#)]
58. Lin, I.-H.; Lu, Y.-H.; Chen, H.-T. Nitrogen-doped carbon nanotube as a potential metal-free catalyst for CO oxidation. *Phys. Chem. Chem. Phys.* **2016**, *18*, 12093–12100. [[CrossRef](#)] [[PubMed](#)]
59. Liu, T.F.; Ali, S.; Li, B.; Su, D.S. Revealing the role of sp²@sp³ structure of nanodiamond in direct dehydrogenation: Insight from DFT study. *ACS Catal.* **2017**, *7*, 3779–3785. [[CrossRef](#)]
60. Zhu, Y.; Lv, K.; Wang, X.; Yang, H.; Xiao, G.; Zhu, Y. 1D/2D nitrogen-doped carbon nanorod arrays/ultrathin carbon nanosheets: Outstanding catalysts for the highly efficient electroreduction of CO₂ to CO. *J. Mater. Chem. A* **2019**, *7*, 14895–14903. [[CrossRef](#)]



© 2020 by the authors. Licensee MDPI, Basel, Switzerland. This article is an open access article distributed under the terms and conditions of the Creative Commons Attribution (CC BY) license (<http://creativecommons.org/licenses/by/4.0/>).